Available online at www.sciencedirect.com

ScienceDirect

Journal of Computational and Applied Mathematics 209 (2007) 66–80

JOURNAL OF COMPUTATIONAL AND APPLIED MATHEMATICS

www.elsevier.com/locate/cam

Determination of a spacewise dependent heat source

Tomas Johansson*, Daniel Lesnic

Department of Applied Mathematics, University of Leeds, LS2 9JT Leeds, UK

Received 5 May 2006

Abstract

This paper investigates the inverse problem of determining a spacewise dependent heat source in the parabolic heat equation using the usual conditions of the direct problem and information from a supplementary temperature measurement at a given single instant of time. The spacewise dependent temperature measurement ensures that the inverse problem has a unique solution, but this solution is unstable, hence the problem is ill-posed. For this inverse problem, we propose an iterative algorithm based on a sequence of well-posed direct problems which are solved at each iteration step using the boundary element method (BEM). The instability is overcome by stopping the iterations at the first iteration for which the discrepancy principle is satisfied. Numerical results are presented for various typical benchmark test examples which have the input measured data perturbed by increasing amounts of random noise.

MSC: 35R25; 47A52; 35K05; 78M15

Keywords: Boundary element method; Discrepancy principle; Heat source; Inverse problem; Iterative regularization; Parabolic heat equation

1. Introduction

The inverse problem of determining an unknown inhomogeneous spacewise dependent heat source function in the heat conduction equation has been considered in a few theoretical papers concerned with the existence and uniqueness of the solution, notably in [1,7,9]. However, as yet no numerical algorithms have been attempted under such rigorous mathematical conditions. In this paper, the determination of the unknown heat source is sought from the usual conditions of the direct problem and a temperature measurement over the domain at a given single instant of time. Although sufficient conditions for the solvability of the inverse problem are provided, see Section 2.3, the problem is still ill-posed since small errors, inherently present in any practical measurement, give rise to unbounded and highly oscillatory solutions. Therefore, in this paper, in order to overcome the instability of the solution, an iterative regularizing algorithm is proposed, see Section 3, which recasts the inverse problem into a sequence of direct problems which are well-posed according to Section 4. These direct problems are solved numerically at each iteration step using the BEM, see Section 7, until a prescribed stopping criterion is satisfied. Convergence of the procedure is given in Section 5. The procedure is applied to the reconstruction of several spacewise dependent heat sources, from infinitely differentiable to discontinuous functions, see Section 8.

* Corresponding author. Tel.: +44 113 343 5182.
E-mail address: amt02tj@maths.leeds.ac.uk (T. Johansson).

0377-0427/$ - see front matter © 2006 Elsevier B.V. All rights reserved.
doi:10.1016/j.cam.2006.10.026

2. Formulation of the inverse problem

2.1. Functional spaces

Let Ω be a bounded domain of $\mathbb{R}^n$, where $n \geqslant 1$, with Lipschitz boundary Γ. The space $L^2(\Omega)$ consists of square integrable functions on Ω with the usual norm $\|\cdot\|_{L^2(\Omega)}$ and scalar product $(\cdot,\cdot)$. The space $H^k(\Omega)$, where $k = 1, 2, \ldots$, denotes the standard Sobolev space on Ω, i.e., the space of functions with generalized derivatives of order $\leqslant k$ in $L^2(\Omega)$. Since the boundary of Ω is Lipschitz the trace of functions in $H^1(\Omega)$ to the boundary is well-defined and $H_0^1(\Omega)$ consists of functions with $u|_\Gamma = 0$.

Let $T > 0$ be a fixed number. The space $L^2(0, T; X)$, where X is a Hilbert space, denotes the space of measurable functions $u(\cdot, t) : (0, T) \to X$, such that

$$\int_\Omega \|u(\cdot, t)\|_X^2 \, \mathrm{d}t < \infty.$$

By $C([0, T]; X)$, we mean functions u such that the mapping $u(\cdot, t) : [0, T] \to X$ is continuous (in the usual norms).

2.2. Assumptions on the differential operator and its semigroup

We assume that

$$Lu = -\sum_{i,j=1}^{n} \partial_{x_i}(a_{i,j}(x)\partial_{x_j} u) + \sum_{i=1}^{n} b_i(x)\partial_{x_i} u + c(x)u, \tag{1}$$

where $a_{i,j} = \bar{a}_{j,i}$ (the bar denotes complex conjugation) and $a_{i,j}, b_i \in C^1(\overline{\Omega})$ and $c \in C(\overline{\Omega})$. Moreover, we suppose that the operator L is elliptic, i.e., there exists a constant C such that

$$\mathrm{Re} \sum_{i,j=1}^{n} a_{i,j}(x)\xi_i\xi_j \geqslant C|\xi|^2$$

for every $x \in \overline{\Omega}$ and all $\xi \in \mathbb{R}^n$. Furthermore, since we can always change u into $\mathrm{e}^{\lambda t}u$, the coefficients are assumed chosen such that there exists a constant $C > 0$ with

$$\mathrm{Re}\, a(u, u) + \lambda\|u\|_{L^2(\Omega)}^2 \geqslant C\|u\|_{H_0^1(\Omega)}^2 \tag{2}$$

for all $u \in H_0^1(\Omega)$ and $\lambda \geqslant 0$, where

$$a(u, v) = \sum_{i,j=1}^{n} \int_\Omega a_{i,j}(x)(\partial_{x_i} u)(\partial_{x_j}\bar{v}) + \sum_{i=1}^{n} \int_\Omega b_i(x)(\partial_{x_i} u)\bar{v} + \int_\Omega c(x)u\bar{v}.$$

We briefly outline that under these assumptions the operator $-L$ generates a contraction semigroup. Let $D(L) = \{u : u \in H_0^1(\Omega), Lu \in L^2(\Omega)\}$. Then, clearly, $D(L)$ is dense in $L^2(\Omega)$ and L is a closed operator. Furthermore, the problem of finding $u \in D(L)$ with

$$Lu + \lambda u = f \quad \text{for } f \in L^2(\Omega),$$

is the equivalent of solving

$$a(u, v) + \lambda(u, v) = (f, v),$$

for every $v \in H_0^1(\Omega)$. Due to (2), this has a unique solution for every $\lambda > 0$, and since $\mathrm{Re}\, a(u, u) \geqslant 0$,

$$\|u\|_{L^2(\Omega)} \leqslant \frac{1}{\lambda}\|f\|_{L^2(\Omega)}.$$

From the Hille–Yosida theorem, see for example [3, Theorem 2.6 in Chapter 1], the operator $-L$ generates a C_0 (continuous) contraction semigroup $\{G(t)\}_{t\in\mathbb{R}^+}$ in $L^2(\Omega)$, so in particular $\|G(t)\| \leqslant 1$. But since $\operatorname{Re} a(u,u) \geqslant C\|u\|^2_{H_0^1(\Omega)}$, it follows that $-L$ is strictly dissipative and hence

$$\|G(T)\| < 1. \tag{3}$$

Moreover, using estimates for the resolvent operator of L, one can show that one can extend $G(t)$ to an analytic semigroup in the right half-plane, see [3, Theorem 4.5 in Chapter 2].

Note that since $H_0^1(\Omega)$ can be compactly embedded into $L^2(\Omega)$, it follows that $G(t)$ is a compact operator for every $t > 0$. We also point out that the above results hold under weaker assumptions on the coefficients, for example the coefficients can be piecewise smooth, corresponding to a layered material.

2.3. The inverse problem and some of its properties

Assume that we have a non-homogenous and non-isotropic body represented by the domain Ω, where Ω is as above. We consider the following inverse problem: find the temperature u and heat source f which satisfy the heat conduction equation in Ω with a space-dependent heat source, namely

$$u_t(x,t) + Lu(x,t) = f(x) \quad \text{for } (x,t) \in \Omega \times (0,T), \tag{4}$$

subject to the Dirichlet boundary condition

$$u(x,t) = h(x,t) \quad \text{for } (x,t) \in \Gamma \times (0,T), \tag{5}$$

(similar analysis can be carried out also for Neumann or mixed boundary conditions), the initial condition

$$u(x,0) = \psi_0(x) \quad \text{for } x \in \Omega, \tag{6}$$

and the overspecified (upper-base) condition

$$u(x,T) = \psi_T(x) \quad \text{for } x \in \Omega. \tag{7}$$

The operator L is given by (1). Under suitable conditions, this inverse problem has a unique solution. Using the trace theorem, it is sufficient to consider the case when $h = 0$ which will be assumed in the remainder of the paper. Using that the operator $-L$ generates a contraction semigroup and (3), we have the following result due to Theorem 1 in [8].

Theorem 1. *Let $h = 0$ and assume that $\psi_0, \psi_T \in H_0^1(\Omega) \cap H^2(\Omega)$. Then the inverse problem* (4)–(7) *has a unique solution among sources $f \in L^2(\Omega)$ and temperatures u with*

$$\int_0^T (\|u_t(\cdot,t)\|^2_{L^2(\Omega)} + \|u(\cdot,t)\|^2_{H^2(\Omega)})\,\mathrm{d}t < \infty.$$

There also exist uniqueness results in Hölder spaces, see [9].

In order to overcome the instability of the inverse problem (4)–(7) with respect to noise in the data (7), we develop an iterative BEM regularizing algorithm, as described in the next section.

3. An iterative algorithm for finding the source term

In what follows, we need the adjoint problem

$$u_t(x,t) + L^*u(x,t) = g(x) \quad \text{for } (x,t) \in \Omega \times (0,T), \tag{8}$$

where

$$L^*u = -\sum_{i,j=1}^{n} \partial_{x_i}(a_{i,j}(x)\partial_{x_j}u) - \sum_{i=1}^{n} \partial_{x_i}(b_i(x)u) + c(x)u.$$

The procedure for the stable reconstruction of the solution u and source term f in (4)–(7) runs as follows:

(i) Choose a function $f_0 \in L^2(\Omega)$. Let u_0 be the solution to (4)–(6) with $f = f_0$.
(ii) Assume that f_k and u_k have been constructed. Let v_k solve (5), (6) and (8) with $g(x) = u_k(x, T) - \psi_T(x)$ and $\psi_0 = 0$.
(iii) Let

$$f_{k+1}(x) = f_k(x) - \gamma v_k(x, T),$$

where $\gamma > 0$, and let u_{k+1} solve (4)–(6) with $f = f_{k+1}$.

The procedure continues by repeating the last two steps until a desired level of accuracy is achieved.

4. Well-posedness of the problems in the iterative procedure

Here, we discuss the well-posedness of the problems used in the iterative procedure given in the previous section. The operator $-L$ generates a contraction semigroup in $L^2(\Omega)$ according to Section 2.2, so we consider (4) in an appropriate weak sense. Using the properties of the contraction semigroup in combination with [5, Chapter 3], we have the following lemma.

Lemma 2. *Let $h = 0$. Suppose that ψ_0 and f belong to $L^2(\Omega)$. Then* (4) *has a unique solution $u \in L^2(0, T; H_0^1(\Omega) \cap C([0, T]; H_0^1(\Omega))$ in the distributional sense which satisfies* (6), *and*

$$\|u\|_{L^2(0,T;H_0^1(\Omega))} \leqslant C(\|f\|_{L^2(\Omega)} + \|\psi_0\|_{L^2(\Omega)}). \tag{9}$$

Note that the boundary condition is satisfied since $u(\cdot, t) \in H_0^1(\Omega)$ for $t \in (0, T)$. Moreover, the restriction $u(x, t_0)$ is well-defined for $0 \leqslant t_0 \leqslant T$, since $u \in C([0, T]; H_0^1(\Omega))$, so especially $u(x, T)$ is well-defined. We have thereby shown that the problem (4)–(6) used in the iterative procedure given in the previous section is well-posed and the restriction of solutions are well-defined. A similar result can be proved for the adjoint problem consisting of the equations (5), (6), and (8).

5. Convergence of the procedure given in Section 3

Let $\{G(t)\}_{t\in\mathbb{R}^+}$ be the semigroup generated by the operator $-L$, see Section 2.2. Moreover, let u be the unique solution to (4)–(6) given by Lemma 2 with initial data $\psi_0 = 0$. We introduce the linear operator $K(t) : L^2(\Omega) \to L^2(0, T; H_0^1(\Omega) \cap C([0, T]; H_0^1(\Omega))$, by

$$K(t)f = \int_0^t G(t - s)f \, \mathrm{d}s. \tag{10}$$

Then the solution u to (4)–(6) is formally given by $u(t) = G(t)\psi_0 + K(t)f$, so finding a solution to the inverse problem is equivalent of solving the operator equation

$$K(T)f = \psi_T - G(T)\psi_0. \tag{11}$$

Note that this recasts the ill-posedness of our inverse problem. Now, according to [5, Section 1.3 of Chapter 3], the semigroup $\{G^*(t)\}_{t\in\mathbb{R}^+}$, where $G^*(t)$ is the adjoint of $G(t)$, is the semigroup generated by $-L^*$. Thus, one can check that $K^*(T)\xi = v(T)$, where v solves (5), (6) and (8) with $\psi_0 = 0$ and $g = \xi$. We are now in a position to prove the following theorem.

Theorem 3. *Let $\psi_0, \psi_T \in L^2(\Omega)$ and let u be the unique solution to the inverse problem according to Theorem* 2.1. *Assume that γ satisfies $0 < \gamma < 1/\|K(T)\|^2$. Let u_k be the kth approximation in the iterative procedure of Section* 3.

Then

$$\lim_{k\to\infty} \|u - u_k\|_{L^2(0,T;H_0^1(\Omega))} = 0 \tag{12}$$

for every function $f_0 \in L^2(\Omega)$.

Proof. From the iterative procedure and the properties of the operator $K(t)$ given above, we have

$$\begin{aligned} f_{k+1} &= f_k - \gamma v_k(x,T) = f_k - \gamma K^*(T)(u_k(x,T) - \psi_T(x)) \\ &= f_k - \gamma K^*(T)(K(T)f_k - (\psi_T - G(T)\psi_0)). \end{aligned}$$

This is precisely the Landweber–Fridman iteration for solving (11), see [4, p. 155]. Now, the sequence f_k converges to f in $L^2(\Omega)$ from the assumption $0 < \gamma < 1/\|K(T)\|^2$. The inequality (9) then implies that u_k converges to u in $L^2(0,T;H_0^1(\Omega))$. □

Note that since the operator $-L$ generates a contraction semigroup, it follows that $\|K(T)\| \leqslant T$, so the procedure is convergent for $0 < \gamma < T^{-2}$. This estimate for γ is far from being sharp.

6. A stopping rule

The procedure proposed in this paper is a regularization method and it therefore works with inexact data. More precisely, consider the case when there is some error in ψ_T in (7), namely

$$\|\psi_T - \psi_T^\delta\|_{L^2(\Omega)} \leqslant \delta, \tag{13}$$

with $\delta > 0$. The elements u_k^δ and f_k^δ, are obtained by using the procedure of Section 3 with data ψ_0 and ψ_T^δ. We do not include errors in the boundary temperature (4) and the initial temperature (5) since the inverse problem is stable with respect to small pertubations in these data.

Given the noise level δ, we can use the discrepancy principle of [6], to obtain a stopping criterion for ceasing the iterations of Steps (ii) and (iii) of the iterative algorithm of Section 3. This suggests choosing the stopping index $k = k(\delta, \gamma)$ as the smallest index for which

$$\|u_k^\delta(\cdot, T) - \psi_T^\delta\|_{L^2(\Omega)} \approx \delta. \tag{14}$$

7. The boundary element method (BEM)

In this section, for simplicity, we briefly describe the BEM for the one-dimensional time-dependent heat equation and therefore let Ω be the interval $(0, \ell)$ and let $L = -\partial_{xx}^2$. Then (4) becomes

$$\frac{\partial u}{\partial t} - \frac{\partial^2 u}{\partial x^2} = f(x) \quad \text{for } (x,t) \in (0,\ell) \times (0,T). \tag{15}$$

By applying Green's formula we can recast Eq. (15) in the integral form

$$\begin{aligned} \eta(x)u(x,t) = &\int_0^t \left[G(x,t,\xi,\tau)\frac{\partial u}{\partial n(\xi)}(\xi,\tau) - u(\xi,\tau)\frac{\partial G}{\partial n(\xi)}(x,t,\xi,\tau) \right]_{\xi=0,\ell} \mathrm{d}\tau \\ &+ \int_0^\ell G(x,t,y,0)u(y,0)\,\mathrm{d}y + \int_0^\ell f(y)\int_0^t G(x,t,\xi,\tau)\,\mathrm{d}\tau\,\mathrm{d}y, \end{aligned} \tag{16}$$

for $(x,t) \in [0,\ell] \times (0,T]$, where $\eta(0) = \eta(\ell) = \frac{1}{2}$, $\eta(x) = 1$ for $x \in \Omega$, n is the outward unit normal to the space boundary $\{0,\ell\} \times [0,T]$, i.e., $n(0) = -1$ and $n(\ell) = 1$, and G is the fundamental solution of the one-dimensional heat

equation, namely,

$$G(x,t,y,\tau)=\frac{H(t-\tau)}{\sqrt{4\pi(t-\tau)}}\mathrm{e}^{-(x-y)^2/(4(t-\tau))},$$

where H is the Heaviside function.

Then the BEM, see [2], based on the boundary integral equation (16) is employed for solving the direct well-posed problems at each iteration of the recursive algorithm described in Section 3.

8. Numerical results and discussion

We have applied the algorithm of the present paper to the reconstruction of several spacewise dependent heat sources, from infinitely differentiable to discontinuous functions $f(x)$. In the four examples presented below, the domain Ω is one dimensional, i.e., an interval $(0,\ell)$ and $T=1$, and we consider homogeneous Dirichlet boundary conditions

$$u(0,t)=0=h_0(t) \quad \text{and} \quad u(1,t)=0=h_1(t) \ \text{ for } t\in[0,1]. \tag{17}$$

The initial condition (6) is given by

$$u(x,0)=\sin(\pi x)=\psi_0(x) \quad \text{for } x\in[0,1]. \tag{18}$$

In order to investigate the stability of the numerical solution, the upper-base data ψ_T in Eq. (7) was perturbed as

$$\psi_T^{\delta}=\psi+\delta, \tag{19}$$

where δ are random variables generated using the NAG routine G05DDF from a Gaussian normal distribution with zero mean and standard deviation equal to $p\max_{x\in[0,1]}|\psi_T(x)|$, where p is the percentage of additive noise which models the errors inherently present in any practical measurement. The value of p was varied from 0% to 20%. The iterations were stopped according to the discrepancy principle (14). The computations were performed in FORTRAN77 double precision on a SGI-workstation. The value of the parameter $\gamma>0$ in the iterative algorithm was varied between 0 and 200. For $\gamma>200$ the algorithm was found divergent for the geometry $(x,t)\in[0,1]\times[0,1]$ and the heat operator considered.

In the figures the following errors are considered:

$$e(k;\gamma;p)=\|\psi_T^{\delta}-\psi_k\|_{L^2((0,1))} \quad \text{(convergence error)}, \tag{20}$$

$$E(k;\gamma;p)=\|f-f_k^{\delta}\|_{L^2((0,1))} \quad \text{(accuracy error)}, \tag{21}$$

where f is the exact analytical source, if available. In the first example such an f is available analytically such that the accuracy of the numerical solution can be assessed. The other three examples do not possess an explicit analytical expression and in these situations the data ψ_T was generated from the solution of the direct problem (15), (17), and (18) when f is known, to which random noise was added as in (19). By adding a quite large amount of random noise in the input data, we avoid committing an "inverse crime".

BEM discretization with $N=20$, 40 or 80 constant boundary elements uniformly distributed on each of the boundaries $\{0\}\times[0,1]$, $\{1\}\times[0,1]$ and $[0,1]\times\{0\}$ were employed and the supplementary condition (7) was also imposed at N internal nodes uniformly distributed on $[0,1]\times\{1\}$.

Example 1. First we try to reconstruct an infinitely differentiable smooth heat source defined by

$$f(x)=2\pi^2\sin(\pi x) \quad \text{for } x\in[0,1]. \tag{22}$$

In this case the direct problem given by Eqs. (15), (17) and (18) with f given by (22) has the analytical solution

$$u(x,t)=(2-\mathrm{e}^{-\pi^2 t})\sin(\pi x) \quad \text{for } (x,t)\in[0,1]\times[0,1]. \tag{23}$$

Based on (23) we obtain the data (7) as given by

$$u(x,1)=(2-\mathrm{e}^{-\pi^2})\sin(\pi x)=\psi_T(x) \quad \text{for } x\in[0,1]. \tag{24}$$

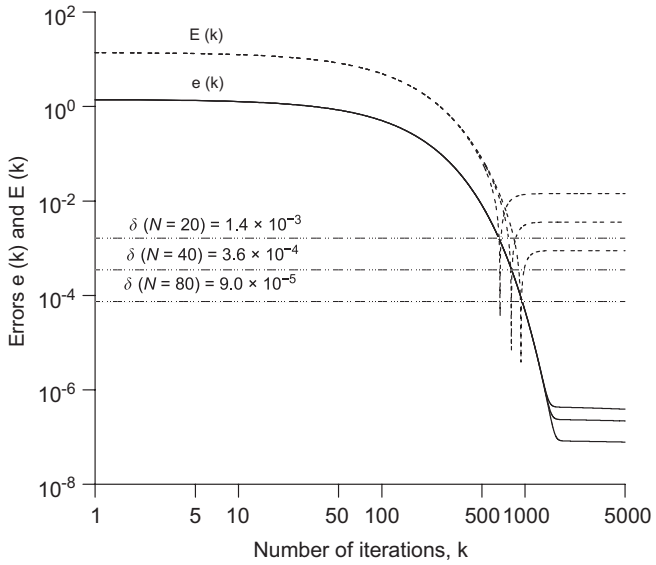

Fig. 1. The errors $e(k)$ and $E(k)$, as functions of the number of iterations k, when $\gamma = 1$, $p = 0$ and various numbers of boundary elements $N \in \{20, 40, 80\}$, for Example 1. The values of $\delta(N) = \|\psi_T - \psi_T(N)\|_{L^2((0,1))}$ are also included.

Fig. 1 shows the errors (20) and (21) for $\gamma = 1$, $p = 0$ and various numbers of boundary elements $N \in \{20, 40, 80\}$. Although the data (24) was not perturbed by random noise, as in (19), the value of δ in (13) depends on N since in the case of exact data, i.e., $p = 0$, $\delta(N) = \|\psi_T - \psi_T(N)\|_{L^2((0,1))}$, where $\psi_T(N)$ is the numerical solution of the direct problem (15), (17) and (18), when f is given by (22). From Fig. 1 the following conclusions can be drawn:

(i) $e_k < E_k$ for all k.

(ii) The accuracy error $E(k)$ possesses a minimum at some iteration number at which the discrepancy principle (14) is first satisfied, i.e.,

$$k = \begin{cases} 670 & \text{for } N = 20, \\ 803 & \text{for } N = 40, \\ 937 & \text{for } N = 80. \end{cases} \tag{25}$$

Up to this level, the error $E(k)$ is independent of N. As k increases beyond this level, it can be seen that $E(k)$ increases and the numerical solution becomes unstable.

(iii) Up to about 2000 iterations the error $e(k)$ is independent of N after which it becomes stationary. This level of stationarity decreases to zero, as the number of boundary elements increases to infinity.

In all of the remainder of the paper, the boundary element mesh was fixed at $N = 40$ and the parameter γ and the percentage amount of noise p were varied.

The measured data ψ_T in (24) was perturbed by $p \in \{1, 3, 5, 10, 20\}\%$ random Gaussian noise with mean zero and standard deviation equal to $(2 - \mathrm{e}^{-\pi^2})p$ which gives

$$\|\psi_T - \psi_T^{\delta}\|_{L^2((0,1))} \approx \delta(p) = \begin{cases} 0.0003 & \text{for } p = 0\%, \\ 0.0079 & \text{for } p = 1\%, \\ 0.0240 & \text{for } p = 3\%, \\ 0.0402 & \text{for } p = 5\%, \\ 0.0805 & \text{for } p = 10\%, \\ 0.1610 & \text{for } p = 20\%, \end{cases} \tag{26}$$

in Eq. (13). According to the discrepancy principle stopping criterion (14) we cease the iterations of the algorithm at the iteration number $k(p, \gamma)$ given in Table 1. The corresponding errors $E(k)$ in predicting the heat source are shown in

Table 1
The stopping iteration number $k(p, \gamma)$ given by (14), with $\delta(p)$ given by (26), for Example 1

$\gamma \backslash p$	0%	1%	3%	5%	10%	20%
1	803	648	539	482	414	347
2	400	323	268	240	206	173
10	77	62	52	46	40	34
100	3	2	2	2	2	2

Table 2
The error $E(k)$ in predicting the heat source at the iteration number $k(p, \gamma)$ given in Table 1

$\gamma \backslash p$	0%	1%	3%	5%	10%	20%
1	3.1E−5	0.0375	0.1149	0.1962	0.3880	0.7601
2	7.3E−5	0.0372	0.1149	0.1956	0.3875	0.7570
10	2.1E−4	0.0366	0.1109	0.1941	0.3760	0.7238
100	3.8E−3	0.0242	0.0615	0.0989	0.1924	0.3795

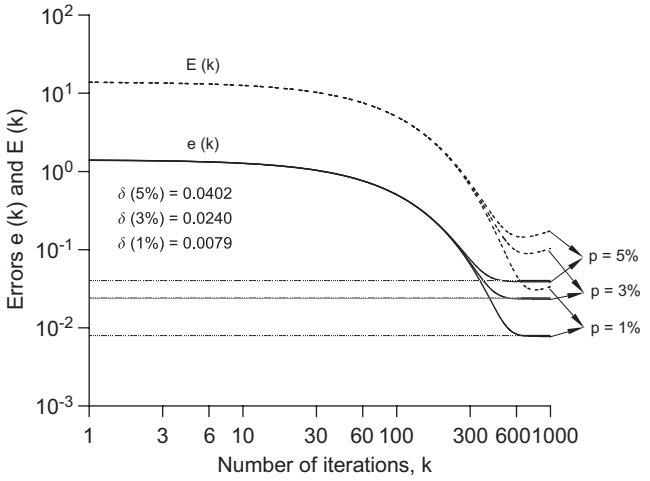

Fig. 2. The errors $e(k)$ and $E(k)$ given by (20) and (21), as functions of the number of iterations k, for various amounts of noise $p = \{1, 3, 5\}\%$ when $\gamma = 1$, for Example 1. The values given by (26) are also included.

Table 2. As expected, as γ or p increases, the attainability of the stopping criterion (14) becomes faster. Surprisingly, the error $E(k)$ decreases as γ increases. The stopping values of k can also be inferred from Fig. 2 which shows the errors $e(k)$ and $E(k)$, as functions of the number of iterations k, for various amounts of noise $p \in \{1, 3, 5\}\%$ obtained with $\gamma = 1$. From this figure it can be seen that the error $e(k)$ decreases as k increases, but the error $E(k)$ starts increasing once

$$k > \begin{cases} 795 & \text{for } p = 1\%, \\ 706 & \text{for } p = 3\%, \\ 662 & \text{for } p = 5\%, \\ 601 & \text{for } p = 10\%, \\ 540 & \text{for } p = 20\%. \end{cases} \tag{27}$$

Then based on (14) with $\delta(p)$ given by (26), one obtains the values for k and $E(k)$ given in Tables 1 and 2 for $\gamma = 1$, respectively.

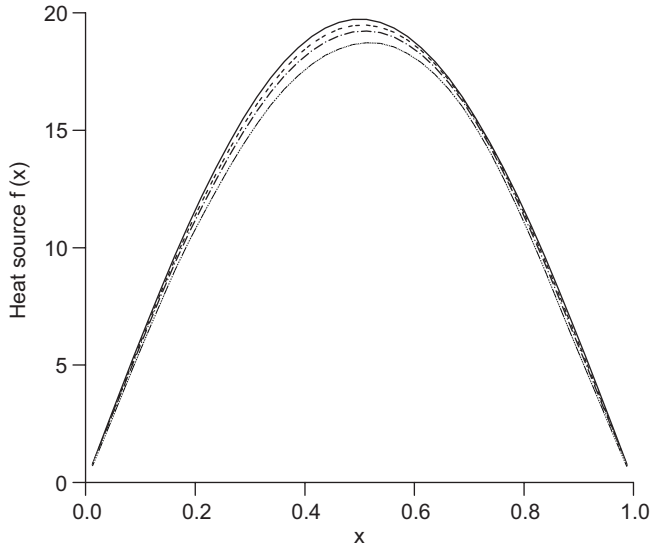

Fig. 3. The analytical solution (22) (——) and the numerical solutions for the heat source, for various amounts of noise $p = 5\%$ (− − −), $p = 10\%$ (− · −) and $p = 20\%$ (− · · · · −), when $\gamma = 1$, for Example 1.

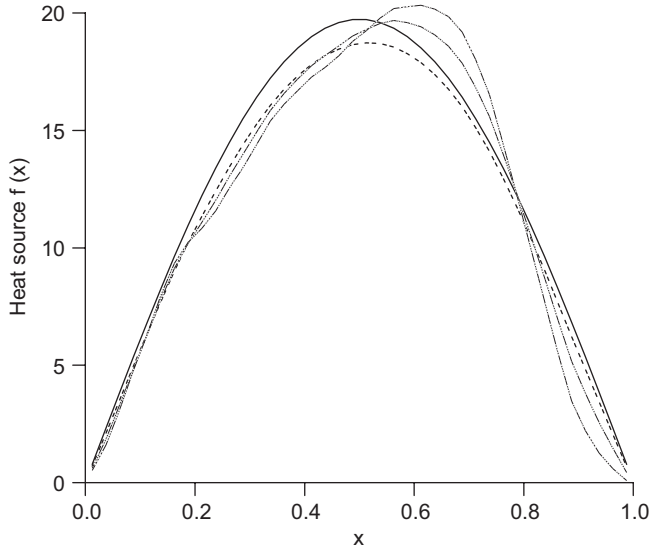

Fig. 4. The analytical solution (22) (——) and the numerical solutions f_k^δ for the heat source for $\gamma = 1$, $p = 20\%$ at various iteration numbers $k = k(\delta) = 347$ (− − −), $k = 5k(\delta)$ (− · ·−) and $k = 10k(\delta)$ (− · · · · −), for Example 1.

Fig. 3 shows the numerical solution of the heat source $f_k^\delta(x)$ at the discrepancy principle iteration k given in Table 1 for $\gamma = 1$, for various percentages of noise $p \in \{5, 10, 20\}\%$ in comparison with the exact solution (22). From Fig. 3 it can be seen that as the amount of noise p decreases, the numerical solution approximates better the exact solution.

In order to indicate the importance of the stopping criterion (14), Fig. 4 shows the numerical solution for the heat source $f_k^\delta(x)$ when $\gamma = 1$, $p = 20\%$ and $k \in \{k(\delta), 5k(\delta), 10k(\delta)\}$, where $k(\delta) = 347$, see Table 1. From this figure, it follows that as $k > k(\delta)$ increases, the numerical solution starts to oscillate and become unstable.

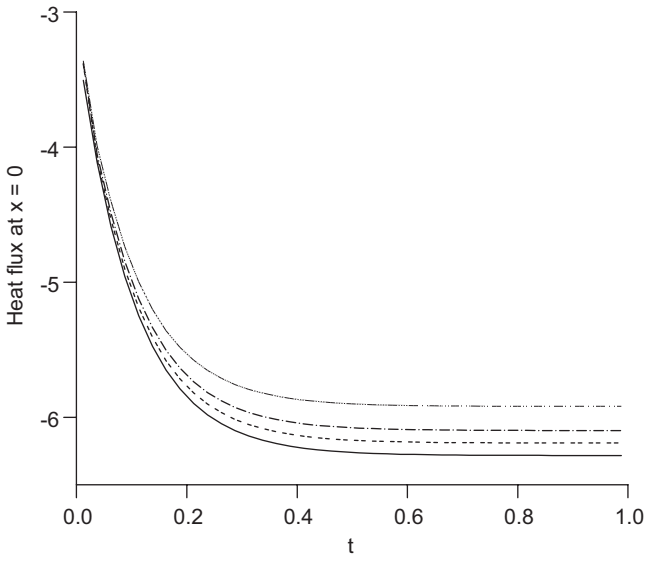

Fig. 5. The analytical solution (28) (——) and the numerical solutions for the heat flux at $x = 0$, for various amounts of noise $p = 5\%$ (− − −), $p = 10\%$ (− · −) and $p = 20\%$ (− · · · · −), when $\gamma = 1$, for Example 1.

Finally, we note that in the post-processing, from Eq. (16), we also obtain the numerical solution for the heat flux $q_k = \partial_n u_k$ at the boundaries $\{0\} \times [0, 1]$ and $\{1\} \times [0, 1]$ and the interior solution $u_k(x, t)$. The heat flux at $x = 0$ is shown in Fig. 5 for various $p \in \{5, 10, 20\}\%$ when $\gamma = 1$ in comparison with the exact solution

$$\partial_n u(0, t) = -\partial_x u(0, t) = \pi(-2 + \mathrm{e}^{-\pi^2 t}) \quad \text{for } t \in [0, 1]. \tag{28}$$

From Fig. 5 one can conclude that the numerical solution approximates better the exact solution as the amount of noise p decreases.

From both Figs. 3 and 5 it can be seen that accurate and stable approximations for the heat source and the heat flux are obtained even for a large amount of noise, such as 20%.

Example 2. We examine the reconstruction of a Gaussian normal distribution

$$f(x) = \frac{1}{\sigma\sqrt{2\pi}} \mathrm{e}^{-(x-\mu)^2/(2\sigma^2)}, \tag{29}$$

where $\mu = 0.5$ is the mean and $\sigma = 0.1$ is the standard deviation. Note that when σ is small expression (29) mimics a Dirac delta distribution $\delta(x - \mu)$. Since the direct problem given by Eqs. (15), (17) and (18) with f given by (29) does not have an analytical solution the data (7) is obtained by solving the direct problem using the BEM. For exact data, i.e., $p = 0$, δ is equal to the machine double-precision of $\mathbf{O}(10^{-16})$ and the iterative process is continued indefinitely.

Fig. 6 shows the numerical solution for the heat source $f_k(x)$ for various values of the iteration number $k \in \{10, 10^2, 10^3, 10^4\}$, when $p = 0$, $\gamma = 100$, in comparison with the exact solution (29). From this figure it can be seen that as k increases the numerical solution f_k converges to the exact solution. However, quite large number of iterations are necessary to achieve convergence even with γ large; for γ smaller even more iterations are required. Parameter free and faster iterative methods such as the conjugate gradient method will be developed in a future work.

Next, the BEM direct problem solution data (7) (which has a maximum absolute value 0.21) is perturbed by Gaussian noise with mean zero and standard deviation equal to $0.21p$ as in (19). This gives

$$\|\psi_T - \psi_T^\delta\|_{L^2((0,1))} \leqslant \delta(p) = \begin{cases} 0.0016 & \text{for } p = 1\%, \\ 0.0050 & \text{for } p = 3\%, \\ 0.0084 & \text{for } p = 5\%, \end{cases} \tag{30}$$

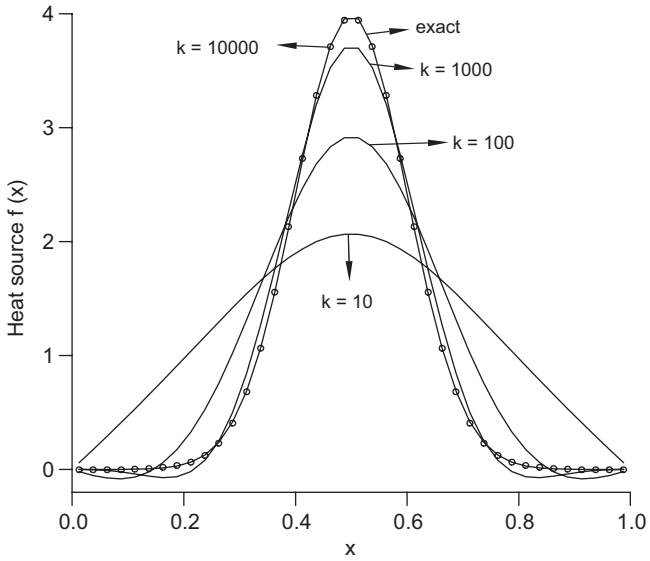

Fig. 6. The numerical solution for the heat source $f_k(x)$ for various values of the iteration number $k \in \{10, 10^2, 10^3, 10^4\}$, when $p = 0$, $\gamma = 100$, in comparison with the exact solution (29), for Example 2.

Table 3
The stopping iteration number $k(p)$ given by (14) with $\delta(p)$ given by (30) and the corresponding error $E(k)$ in predicting the heat source, when $\gamma = 100$, for Example 2

	$p = 1\%$	3%	5%
k	245	113	79
$E(k)$	0.3472	0.4784	0.5602

in Eq. (13). According to the discrepancy principle (14) we cease the iterations of the algorithm at the iteration number $k(p)$ given in Table 3 when $\gamma = 100$. The corresponding errors $E(k)$ are also included in this table. As expected, as p increases, the attainability of the stopping criterion (14) becomes faster. The stopping values of k can also be inferred from Fig. 7 which shows the errors $e(k)$ and $E(k)$, as functions of the number of iterations k, for various amounts of noise $p \in \{0, 3, 5, 10, 20\}\%$ obtained with $\gamma = 100$. From this figure, it can be seen that for exact data, i.e., $p = 0$, both errors keep continuously decreasing to zero as $k \to \infty$. For noisy data, i.e., $p > 0$, the error $e(k)$ decreases as k increases but the error $E(k)$ starts increasing once

$$k > \begin{cases} 1461 & \text{for } p = 1\%, \\ 172 & \text{for } p = 3\%, \\ 119 & \text{for } p = 5\%. \end{cases} \tag{31}$$

Then based on (14) with $\delta(p)$ given by (30), one obtains the values of k and $E(k)$ given in Table 3.

Fig. 8 shows the numerical solution for the heat source $f_k^{\delta}(x)$ at the discrepancy principle iteration k given in Table 3 for various percentages of noise $p \in \{0, 1, 3, 5\}\%$ in comparison with the exact solution (29). From this figure one can conclude that as the amount of noise p decreases, the numerical solution approximates better the exact solution and it is stable for all p, although the accuracy achieved is not as good as that obtained in Example 1. A closer inspection of Fig. 7 shows that if one chooses the optimal iteration stop given by (31) then the errors $E(k)$ decrease in comparison with the values given in Table 3, and they are 0.2330, 0.4570 and 0.5315 for $p = 1\%$, 3% and 5%, respectively. However, this improvement is only significant for relatively low amounts of noise of about 1%.

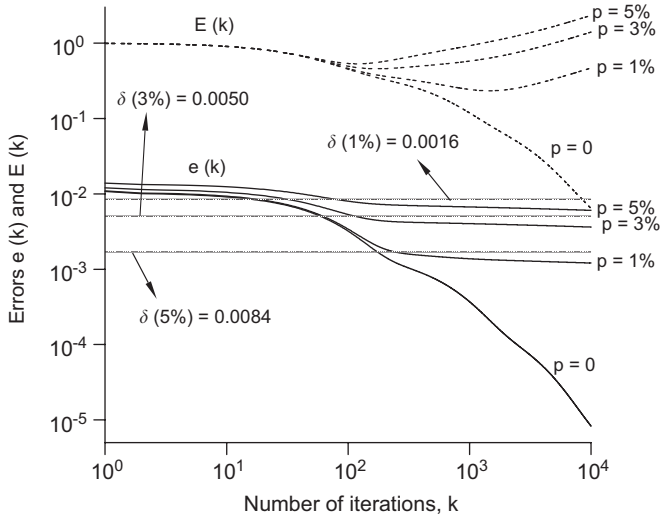

Fig. 7. The errors $e(k)$ and $E(k)$ given by (20) and (21), as functions of the number of iterations k, for various amounts of noise $p = \{0, 1, 3, 5\}\%$ when $\gamma = 100$, in Example 2. The values of $\delta(p)$ given by (30) are also included.

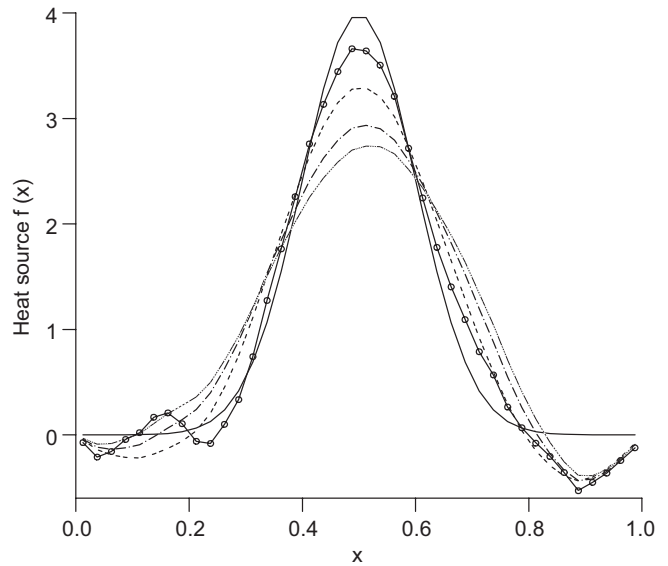

Fig. 8. The exact solution (29) (——) and the numerical solutions for the heat source, for various amounts of noise $p = 0$ $(-\circ-)$ and $k = 10^4$, $p = 1\%$ $(---)$, $p = 3\%$ $(-\cdot-)$ and $p = 5\%$ $(-\cdots-)$, when $\gamma = 100$, for Example 2.

Example 3. In this example, we reconstruct a continuous piecewise smooth heat source, namely

$$f(x) = \begin{cases} 0 & \text{for } 0 \leqslant x < \frac{1}{3}, \\ 6x - 2 & \text{for } \frac{1}{3} \leqslant x \leqslant \frac{1}{2}, \\ 4 - 6x & \text{for } \frac{1}{2} < x \leqslant \frac{2}{3}, \\ 0 & \text{for } \frac{2}{3} < x \leqslant 1. \end{cases} \tag{32}$$

Table 4
The stopping iteration number $k(p)$ given by (14) with $\delta(p)$ given by (33) and the corresponding error $E(k)$ in predicting the heat source, when $\gamma = 100$, for Example 3

	$p = 1\%$	3%	5%
k	689	136	91
$E(k)$	0.0811	0.1387	0.1548

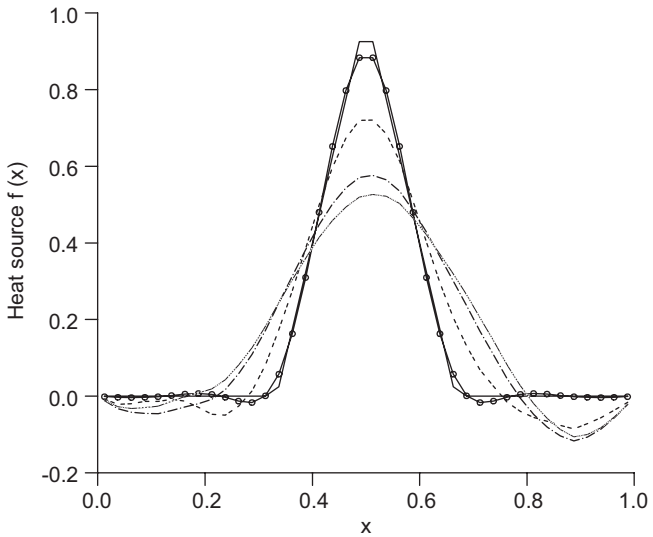

Fig. 9. The exact solution (32) (——) and the numerical solutions for the heat source, for various amounts of noise $p = 0$ ($-\circ-$) and $k = 10^4$, $p = 1\%$ ($- - -$), $p = 3\%$ ($- \cdot -$) and $p = 5\%$ ($- \cdots -$), when $\gamma = 100$, for Example 3.

The BEM direct problem solution data (7) (which has a maximum absolute value 0.037) is perturbed by Gaussian random noise with mean zero and standard deviation equal to $0.037p$ as in (19). This gives

$$\|\psi_T - \psi_T^\delta\|_{L^2((0,1))} \leqslant \delta(p) = \begin{cases} 0.0002 & \text{for } p = 1\%, \\ 0.0008 & \text{for } p = 3\%, \\ 0.0014 & \text{for } p = 5\%, \end{cases} \tag{33}$$

in Eq. (13). According to the discrepancy principle (14), we cease the iterations of the algorithm at the iteration number $k(p)$ given in Table 4 when $\gamma = 100$. The corresponding errors $E(k)$ are included in this table.

Fig. 9 shows the numerical solution for the heat source $f_k^\delta(x)$ at the discrepancy principle iteration k given in Table 4 for the various percentages of noise $p \in \{0, 1, 3, 5, \}\%$ in comparison with the exact solution (32). From Figs. 8 and 9 it can be seen that whilst stable, the numerical solution for Example 3 is less accurate than that of Example 2, as expected since example (32) is less regular than (29). Further, by comparing Figs. 6 and 9 for $p = 0$ it can be seen that for Example 3 even 10 000 iterations are not enough to achieve the full convergence.

Example 4. The last example involves reconstructing a discontinuous heat source given by

$$f(x) = \begin{cases} 0 & \text{for } 0 \leqslant x < \frac{1}{3}, \\ 1 & \text{for } \frac{1}{3} \leqslant x \leqslant \frac{2}{3}, \\ 0 & \text{for } \frac{2}{3} < x \leqslant 1. \end{cases} \tag{34}$$

Table 5
The stopping iteration number $k(p)$ given by (14) with δ given by (35) and the corresponding error $E(k)$ in predicting the heat source, when $\gamma = 100$, for Example 4

	$p = 1\%$	3%	5%
k	209	113	91
$E(k)$	0.1916	0.2115	0.2286

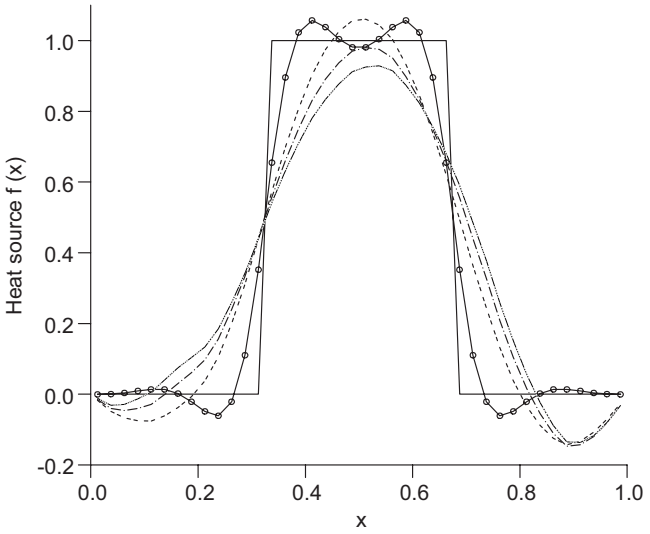

Fig. 10. The exact solution (34) (——) and the numerical solutions for the heat source, for various amounts of noise $p = 0$ $(- \circ -)$ and $k = 10^4$, $p = 1\%$ $(- - -)$, $p = 3\%$ $(- \cdot -)$ and $p = 5\%$ $(- \cdots -)$, when $\gamma = 100$, for Example 4.

The BEM direct problem solution data (7) (which has a maximum absolute value 0.073) is perturbed by Gaussian random noise with mean zero and standard deviation equal to $0.073p$ as in (19). This gives

$$\|\psi_T - \psi_T^\delta\|_{L^2((0,1))} \approx \delta(p) = \begin{cases} 0.0005 & \text{for } p = 1\%, \\ 0.0017 & \text{for } p = 3\%, \\ 0.0029 & \text{for } p = 5\%, \end{cases} \tag{35}$$

in Eq. (13). Corresponding to Table 4 and Fig. 9, we have Table 5 and Fig. 10. The same conclusions as those of Example 3 can be drawn with the note that the oscillatory behaviour near the discontinuities $x = \frac{1}{3}$ and $\frac{2}{3}$ in Fig. 10 for $p = 0$ resembles the well-known Gibbs phenomenon.

9. Conclusions

In this paper a convergent and stable solution of a spacewise dependent heat source has been obtained using an iterative regularizing algorithm. Both theoretical and numerical studies have been provided.

Future work will involve: (i) numerical BEM implementation in higher dimensions; (ii) determination of both spacewise dependent heat source and the initial temperature from the temperature measurements at two different instants; (iii) development of parameter free and faster iterative methods such as the conjugate gradient method; (iv) extensions to the inverse source problems for the wave and plate equations.

Acknowledgement

T. Johansson would like to acknowledge the Grant and financial support from the Wenner–Gren foundations. Both authors would like to thank L. Elliott, A. Farcas and D. B. Ingham for their useful comments on this work.

References

[1] J.R. Cannon, Determination of an unknown heat source from overspecified boundary data, SIAM J. Numer. Anal. 5 (1968) 275–286.
[2] A. Farcas, D. Lesnic, The boundary-element method for the determination of a heat source dependent on one variable, J. Eng. Math. 2006, in press.
[3] J.A. Goldstein, Semigroups of Linear Operators and Applications, Oxford Mathematical Monographs, Oxford, 1985.
[4] H.W. Engl, M. Hanke, A. Neubauer, Regularization of Inverse Problems, Kluwer Academic Publishers Group, Dordrecht, 1996.
[5] J.-L. Lions, E. Magenes, Non-homogeneous Boundary Value Problems and Applications, vol. I, Springer, Berlin, 1972.
[6] V.A. Morozov, On the solution of functional equations by the method of regularization, Dokl. Akad. Nauk SSSR 167 (1966) 510–512 English transl.: Soviet Mathematics Doklady 7 (1966) 414–417.
[7] A.I. Prilepko, V.V. Solov'ev, Solvability theorems and Rothe's method for inverse problems for a parabolic equation, Differential Equations 23 (1988) 1341–1349.
[8] W. Rundell, Determination of an unknown non-homogeneous term in a linear partial differential equation from overspecified boundary data, Appl. Anal. 10 (1980) 231–242.
[9] V.V. Solov'ev, Solvability of the inverse problems of finding a source, using overdetermination on the upper base for a parabolic equation, Differential Equations 25 (1990) 1114–1119.